19th International Conference on Renewable Energies and Power Quality (ICREPQ'21)
Almeria (Spain), 28th to 30th July 2021
Renewable Energy and Power Quality Journal (RE&PQJ)
ISSN 2172-038 X, Volume No.19, September 2021

Modelling of a Permanent Magnet Synchronous Motor and its Control Circuit in Simulink Environment

Mihály Katona[1], Péter Kiss[1]
[1]Department of Electric Power Engineering
Budapest University of Technology and Economics
Budapest, Egry József u. 18, 1111
e-mail: katona.mihaly@edu.bme.hu, kiss.peter@vik.bme.hu

Abstract: The most commonly used electric motor in electric vehicles is the permanent magnet synchronous motor. The primary production and refinement of rare earth materials used in these motors are immensely damaging to the environment. A new wave of technology in the aspect of electric motors is emerging and that is the non-rare earth element magnet assisted synchronous reluctance motor. During the development process it is beneficial to keep the expenditures at the minimum. To reach that goal a comprehensive simulation of the designed motor and its control circuit could be the answer. It is reasonable to use software based on finite element calculations such as FEMM and mathematical simulations as Matlab Simulink. By implementing the equations and methods described in this paper the electric powertrain can be created generally. The specification is highly dependent on the input parameters that are extracted from finite element 2D calculations. In this case, the model approximates the expected behaviour of the investigated construction. A complete driving cycle can be examined, operating points can be determined, and the efficiency map can be created to help the research.

Keywords: simulation, synchronous motor, motor control, electric powertrain

1. Introduction

Nowadays, e-mobility is gaining ground in the fields of passenger transport, mainly because of the reduced environmental pollution those offer. [1] According to authoritative market analysis, such a large increase in demand, combined with the raw material needs of other technical industries, will cause a serious problem in the rare earth market that can be seen already. The goals of the electric vehicle and motor manufacturers are to maximize the profitability of the product while the environmental impact is kept at minimum. The primary production and refinement of rare earth materials are immensely damaging to the environment. The share of permanent magnets in the market of rare earth materials is immensely significant. It is nearly 40% by volume and it overwhelms the market by more than 90% in the aspect of value. [2] This market situation demand puts pressure on the manufacturers to reduce the costs of the powertrain, engine design and development. We hope that the hardware performance and computing capacity of the modern computers and the implementation of the already formulated mathematical models provide an opportunity to approximate the behaviour of the powertrain of a newly designed motor concept. The mathematical models in a Simulink environment make it possible to observe the expected operation of the design during digital phase of the product development process. This frees up the project from significant expenditures, thus helping its economic competitiveness. The main objectives are to approximate the accuracy of the control, to investigate the system response to variable load and control signal, to determine how close the torque characteristic of the motor to the reference is.

2. Mathematical modelling

A. Connection to finite element calculation

To approximate the input parameters of the analytical model presented in this section a simulation process from the topology building to the evaluation and display of the results were created, the program code was developed in Matlab software extended with OctaveFEMM software package, which uses the Lua programming language which FEMM can understand. The created software code is eligible to calculate the following parameters as a function of current, load angle and so on: torque, direct flux linkage, quadrature flux linkage, direct inductance, quadrature inductance, pole flux, resistance. The method used to calculate these parameters on a given topology and the results will be presented in a further article.

B. *Direct and quadrature parameters*

A reasonable choice is to use the orthogonal coordinate system, where the direct component (d) is fixed to the pole flux vector of the rotor, relative to which the quadrature direction (q) differs by an electrical angle of 90°. In this case, it is not necessary to use trigonometric equations to describe electric parameters. Furthermore, the direct and quadrature components give a constant result over time, so that the waveforms of the electrical values associated with the operation of the motor are converted into a constant signal in the case of an ideal sinusoidal supply. Thus, during the modelling, the mathematical equations describe the operation of the control circuit with direct and quadrature components, but the sensors in a finished product provide the input parameters of the program code in time-based values as in the simulation, so it is necessary to transform them into the orthogonal coordinate system for the program code to use.

In case of Clarke transformation, the a-b-c components of the measured three-phase values are transformed into the α-β-0 reference frame, where the components have a phase difference of 90° and the zero-order component value is zero. The transformation and inverse transformation matrices are described by Equations (1) and (2). [3]

$$\begin{bmatrix} f_\alpha \\ f_\beta \\ f_0 \end{bmatrix} = \begin{bmatrix} \frac{2}{3} & -\frac{1}{3} & -\frac{1}{3} \\ 0 & \frac{1}{\sqrt{3}} & -\frac{1}{\sqrt{3}} \\ \frac{1}{3} & \frac{1}{3} & \frac{1}{3} \end{bmatrix} \cdot \begin{bmatrix} f_a \\ f_b \\ f_c \end{bmatrix} \quad (1)$$

$$\begin{bmatrix} f_a \\ f_b \\ f_c \end{bmatrix} = \begin{bmatrix} 1 & 0 & 1 \\ -\frac{1}{2} & \frac{\sqrt{3}}{2} & 1 \\ -\frac{1}{2} & -\frac{\sqrt{3}}{2} & 1 \end{bmatrix} \cdot \begin{bmatrix} f_\alpha \\ f_\beta \\ f_0 \end{bmatrix} \quad (2)$$

In case of Park transformation, the stationary coordinate system with the α-β-0 reference frame is transformed into a co-rotating coordinate system consisting of d-q-0 components. The direct component (d) is the same as the direction of the pole flux of the rotor. The transformation and inverse transformation matrices are described by Equations (3) and (4).

$$\begin{bmatrix} f_d \\ f_q \\ f_0 \end{bmatrix} = \begin{bmatrix} \cos(\varphi_e) & \sin(\varphi_e) & 0 \\ -\sin(\varphi_e) & \cos(\varphi_e) & 0 \\ 0 & 0 & 1 \end{bmatrix} \cdot \begin{bmatrix} f_\alpha \\ f_\beta \\ f_0 \end{bmatrix} \quad (3)$$

$$\begin{bmatrix} f_\alpha \\ f_\beta \\ f_0 \end{bmatrix} = \begin{bmatrix} \cos(\varphi_e) & -\sin(\varphi_e) & 0 \\ \sin(\varphi_e) & \cos(\varphi_e) & 0 \\ 0 & 0 & 1 \end{bmatrix} \cdot \begin{bmatrix} f_d \\ f_q \\ f_0 \end{bmatrix} \quad (4)$$

where,

φ_e the rotor position in electrical angle [rad]

C. Electrical and mechanical properties

The sinusoidal distribution of the magnetic field generated by the permanent magnets of the synchronous machine can be described by the pole flux vector, i.e. it can be said that the flux of the rotor is equal to the pole flux vector. [4]

$$\bar{\Psi}_{rotor} = \bar{\Psi}_p \quad (5)$$

where,

Ψ_p pole flux [Vs]

The stator terminal voltage can be described as the sum of the pole voltage and the voltage across the winding.

$$\bar{V}_t = R\bar{\imath} + \bar{L}\frac{d\bar{\imath}}{dt} + j\omega_e\bar{L}\bar{\imath} + j\omega_e\bar{\Psi}_p \quad (6)$$

$$\omega_e = p\omega_m \quad (7)$$

where,

ω_e rotor electrical rotation speed [rad/sec]
ω_m rotor mechanical rotation speed [rad/sec]
p rotor pole pair number [u.]

The real part of Equation (6) gives the direct (d) values of the motor, while the imaginary part gives the quadrature (q) components, as Equations (8) and (9) show. The currents are expressed from the latter equations, since during the simulation the control signal will be the voltage as the feedback is provided by the current. [5]

$$\frac{di_d}{dt} = -\frac{R}{L_d}i_d + \frac{\omega_e L_q}{L_d}i_q + \frac{1}{L_d}V_d \quad (8)$$

$$\frac{di_q}{dt} = -\frac{R}{L_q}i_q - \frac{\omega_e L_d}{L_q}i_d + \frac{1}{L_q}V_q - \frac{\omega_e\Psi_p}{L_q} \quad (9)$$

where,

i_d, i_q current of the stator [A]
L_d, L_q inductance of the stator [H]
V_d, V_q terminal voltage of the stator [V]
R resistance of the stator [Ω]

It is clear from Equations (8) and (9) that the direct (d) and quadrature (q) components are interdependent, so it is worthwhile to integrate the equations in a discrete range, where the next element (k) is always derived from the preceding element (k-1). The torque depends on the pole flux and the current vector described by equation (8).

$$T = \frac{3}{2}p|\bar{\Psi} \times \bar{\imath}| = \frac{3}{2}p\left(\Psi_p i_q + \left(L_d - L_q\right)i_q i_d\right) \quad (10)$$

The rotor speed can be calculated by the mechanical equation of a parallel spring and a mass.

$$\mathrm{M}(\varphi) = \Theta\ddot{\varphi} + D\dot{\varphi} + K\varphi \quad (11)$$

where,

θ moment of inertia [kgm^2]
D damping factor [Nms]
K torsion factor [Nm/rad]

The solution of the equation is the transfer function between the angular velocity and the torque, which is written as Laplace transformant. Rearranging Equation (11), where the angular velocity is the time derivative of the angular rotation, which is equivalent to be multiplied by ***s*** in the Laplace range. The transfer function is given by Equation (12).

$$Y = \frac{\omega_m}{M} = \frac{s}{\Theta s^2 + Ds + K} \quad (12)$$

When calculating the speed, it is not necessary to delay the input signals, since the torque is calculated from the already delayed (k-1) element. At a sufficiently high resolution, this delay prevents the formation of computational loops and does not cause a stability problem later. Implementing the equations described in this chapter and using appropriate transformations, the PMSM model can be constructed.

3. Field-oriented pulse width modulation

Motor control using space vectors is a field-oriented modulation technique where the carrier signal is compared with a high frequency sawtooth modulator signal. The number of pulses per cycle is given by the relative deviation of the frequency and amplitude of the modulating signal and the carrier signal. Due to the design of the inverter, two transistors on three bridges define 8 different switch states. During the modelling, I implemented a simple two-level inverter where one bridge can be connected to either the positive or the negative rail. Apart from the offset and losses, the maximum of the motor phase voltage can be half the DC voltage of the inverter.

$$V_e = \frac{V_{DC}}{2} \quad (13)$$

where,

V_{DC} DC inner voltage of the inverter [V]
V_e DC rail voltage of the inverter [V]

As a three-phase symmetrical excitation, the impedance of each phase coil is the same $|\bar{Z}_a| = |\bar{Z}_b| = |\bar{Z}_c|$. The sum of the phase voltages is also zero $\bar{U}_{aY} + \bar{U}_{bY} + \bar{U}_c Y = 0$. The voltage at the star point relative to ground is equal to the zero-order voltage described by Equation (14) if two bridge branches are connected to a positive rail. [6]

$$V_0 = \frac{V_a + V_b + V_c}{3} = \frac{V_e + V_e + (-V_e)}{3} \quad (14)$$

where,

V_0 zero order voltage [V]

V_a, Vb, Vc phase voltages [V]

Based on the latter the maximum voltage of a phase:

$$V_{f0} = V_a + V_0 = \frac{1}{3}V_e + V_e = \frac{4}{3}V_e \quad (17)$$

If the switching states are examined in a stationary coordinate system, we get the result shown in Figure 2, where a 3-bit tag represents the different switch states, with 0 denoting that the bridge is connected to negative rail, whilst 1 denoting the positive state. In order to facilitate the control, it is worth setting the inner circuit shown in Figure 2 as a limit voltage.

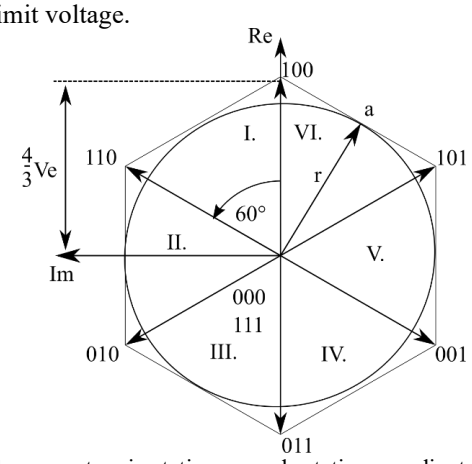

Fig. 2. Space vectors in stationary and rotating coordinate system

It can be clearly seen that the absolute value of the output voltage vector is equal to the radius of the inner circle, which is the height of the sector. This can be calculated by the height formula of a triangle.

$$rV_e = \frac{1}{2}a \cdot cot\frac{\pi}{n} = \frac{1}{2} \cdot cot\frac{\pi}{6} = \frac{\sqrt{3}}{2}V_e \quad (15)$$

where,

r radius of the inscribed circle [p.u.]

a length of one side of the hexagon [p.u.]

n number of sides of the hexagon [p.u.]

During the coding of the model, it is important to determine the maximum of the phase voltage which is described by equation (16).

$$V_{f|max} = V_{f0}r = \frac{4}{3} \cdot \frac{\sqrt{3}}{2} \cdot \frac{1}{2}V_{dc} = \frac{1}{\sqrt{3}}V_{dc} \quad (16)$$

In the model the output signals of the inverter vary between $\pm V_{f|max}$. Of the three pulse width modulation types - edge, centre and adaptive - the implementation of the first was done. In the case of simulations running only in a digital environment, no significant difference in the results was observed. In the case of the HIL test, it is advisable to use adaptive fitting depending on the current measurement method. In the case of edge-aligned modulation, the modulator signal is a high-frequency sawtooth signal (16-20kHz) while the carrier is a sine wave.

$$C = \begin{cases} 1, if\ J_m \le J_c \\ 0, if\ J_m > J_c \end{cases}, where\ J_m, J_c \in [0,1] \quad (17)$$

where,

C control signal of the inverter bridges [p.u.]

J_m modulator signal [p.u.]

J_c carrier signal [p.u.]

The formation of an arbitrary voltage vector in a sector is determined by the relative on-time of the two vectors enclosing that sector and the zero vectors. The design of the control is such that the possibility of double switching is avoided to reduce the number of switches of the transistors and to increase their operation time. It means that switching only one bridge at a time to move between two consecutive states should be sufficient. [6]

1. Table. Switching sequence in case of svPWM [6]

vector (v)	1	2	7	2	1	8	1	2	7
cycle (T_c)	T_c			T_c+1			T_c+2		

2. Table. Vector identifiers in case of svPWM [6]

vector (v)	**State of bridges (h)**		
	A	**B**	**C**
1	1	0	0
2	1	1	0
3	0	1	0
4	0	1	1
5	0	0	1
6	1	0	1
7	1	1	1
8	0	0	0

sector (s)	**Enclosing vectors (v)**		
	1.	**2.**	**3.**
1	1	2	7,8
2	2	3	7,8
3	3	4	7,8
4	4	5	7,8
5	5	6	7,8
6	6	1	7,8

To determine the modulator signal, it is necessary to calculate the angular position of the d-q coordinate system rotating with the pole flux vector, which is given by the integration of the electrical angular velocity. In addition, the angular position of the voltage vector determined by the control circuit is also essential. Using these values, the relative on-time of an enclosing vector can be calculated in a cycle. [6] The angular position of the control voltage is shown in Figure 3.

$$\theta_{xV} = \theta_{dV} + \theta_{xd} \quad (18)$$

$$b_{v1} = \frac{\sqrt{3}V}{V_{DC}} \sin\left(\frac{\pi}{3} - \theta_{xV}\right) \quad (19)$$

$$b_{v2} = \frac{\sqrt{3}V}{V_{DC}} \sin\left(\theta_{xV}\right) \quad (20)$$

$$b_{v3} = 1 - b_{v1} - b_{v2} \quad (21)$$

where $\theta_{xd} = \varphi_e$,

b_{v1}, b_{v2}, b_{v3} relative on-time [p.u.]

V absolute value of the control vector [V]

θ_{xV} angular position of the control vector [rad]

θ_{dV} angular position of the voltage vector in d-q [rad]

θ_{xd} angular position of the d-q reference frame [rad]

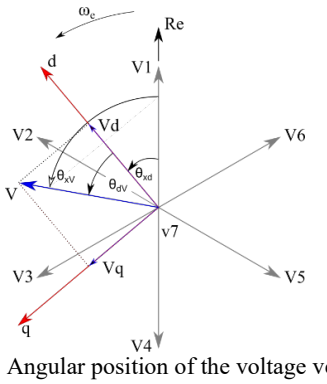

Fig. 3. Angular position of the voltage vector

The angular position of the control vector defines the sector. Equations (18) - (21) are normalized to one sector, so it is necessary to divide the angular position of the control vector by sixty with remainder. Next, it is advisable to structure the program code by selecting enclosing vectors (v) for the sector input parameter (s) based on Table 2. The output values are three-element vectors containing the state of the bridges. Multiplying them by their relative on-time results the actual on-time of one bridge. In case of the null vector, it is necessary to take half of the relative on-time due to the equality of the vectors [1 1 1] and [0 0 0]. One possible output of the program code is:

$$b_{hA} = \begin{bmatrix}1\\0\\0\end{bmatrix} b_{v1} \quad b_{hB} = \begin{bmatrix}1\\1\\0\end{bmatrix} b_{v2} \quad b_{hC} = \begin{bmatrix}1\\1\\1\end{bmatrix} b_{v3} \tag{22}$$

$$J_{mA} = b_{hA}(1)b_{v1} + b_{hB}(1)b_{v2} + b_{hC}(1)\frac{b_{v3}}{2} \tag{23}$$

$$J_{mB} = b_{hA}(2)b_{v1} + b_{hB}(2)b_{v2} + b_{hC}(2)\frac{b_{v3}}{2} \tag{24}$$

$$J_{mC} = b_{hA}(3)b_{v1} + b_{hB}(3)b_{v2} + b_{hC}(3)\frac{b_{v3}}{2} \tag{25}$$

where,

b_{hA}, b_{hB}, b_{hC}	on-time of enclosing vector [p.u.]
J_{mA}, J_{mB}, J_{mC}	on-time of inverter bridge [p.u]

The control circuit is designed as a simple two-stage regulator, with a speed and current controller connected in series in normal and field weakening operation for quadrature (q) current. In electric vehicles it is rare to measure back the torque of the motor so that regulator is unnecessary.

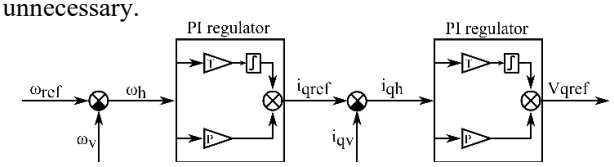

Fig. 4. Two-stage, serial PI regulators

The transformation of the measured current is also necessary here, so that the control can take place in the d-q coordinate system. During tuning, the value of the proportional coefficient can be taken as one first. The integral coefficient of the current controller can be approximated by the electrical time constant and in case of the speed controller, by the mechanical time constant of the motor. Neglecting the field weakening operation, it can be assumed that the value of the direct component (d) of the current is zero as a reference value. The operation in field weakening is defined by the following. As the motor reaches the maximal rotation speed at the maximal voltage assuming that the value of the direct current is zero, there could be a possible need to increase the rotational speed. Following the theory used in normal operation it assumes that as the rotational speed increases the terminal voltage either. This is not possible, so the weakening of the motor flux is used to reach higher speed values. Rearranging Equation (9) it shows exactly the connection mentioned beforehand. [7]

$$\frac{di_q}{dt} = -\frac{R}{L_q} i_q - \omega_e\left(\frac{L_d}{L_q} i_d + \frac{\Psi_p}{L_q}\right) + \frac{1}{L_q} V_q \tag{26}$$

Equation (26) defines that the $-\frac{\omega_e \Psi_p}{L_q}$ component restricts the maximum value of the quadrature current depending on the rotation speed since the direct currents value is zero. That restriction comes from the voltage induced by the permanent magnets. It is possible to compensate the effect via $-\frac{\omega_e L_d}{L_q} i_d$ component, where the value of the direct current tends to negative. If the current control is defined as a vector, it is possible to interpret the equation by rotating the control vector so that way the direct component is negative as the phase angle of the control vector is 90° at first. The field weakening algorithm defines the phase angle between $90° < \varphi_{FW} < \varphi_{max}$ where the maximal angle is defined considering safety factors, usually less than 180°.

The rotation speed control in field weakening operation is the same as in normal operation except the tuning of the PI regulator. The input parameters of the current control are the same as well. To ensure that the initial control vectors phase angle is 90° and its amplitude is equal to the maximum of the normal operation the reference direct current is zero and the quadrature component is provided by the rotation speed regulator. Note that a transformation is needed from d-q components to polar coordinates. To sense the change in the operation it is appropriate to use the control voltage vectors direct and quadrature components, so those are additional input parameters. The weakening factor is defined by the following Equation (27). [7]

$$M = \frac{\sqrt{V_q^2 + V_d^2}}{V_{DC}} \tag{27}$$

where,

M	field weakening factor [p.u.]

It is required to define a threshold that ensures that the decrease of the current control amplitude happens in field weakening operation only, but it is recommended to use a threshold value less than 1 to create a transition between the two operation fields. The weakening factor is controlled by a PI regulator. The topology is shown in Figure 5.

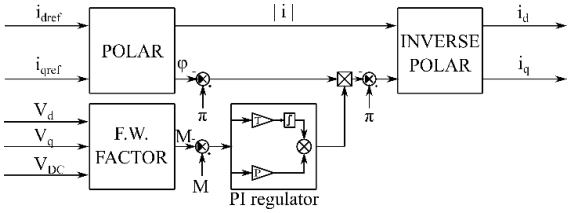

Fig. 5. Topology of the field weakening

During the PI regulator tuning the following effects of the parameters were taken into consideration.

$$G_{PI}(s) = K_P + \frac{1}{T_I s} \tag{28}$$

where,

G_{PI}	gain of the control circuit [p.u.]
K_P	proportional coefficient of the control circuit [u.]
T_I	integral coefficient of the control circuit [u.]

The effect of increasing the parameters mentioned above is summarized in Table 3.

3. Table. The effect of increasing control parameters

	t_{rise}	$A_{overshoot}$	t_{settle}	A_{error}
K_P	decrease	increase	-	decrease
$1/T_I$	decrease	increase	increase	eliminate

An appropriate method for tuning the control circuit is the Good Gain method formulated by Finn Haugen or the well-known Ziegler-Nichols method. [8,9]

4. Results

To approximate the accuracy of the control circuit, to investigate the system response to variable load and control signal and to determine how close the torque characteristic of the motor to the reference is, I created an additional fine-tuned control circuit model in Matlab Simulink, beside the motor and inverter model. The system was loaded by different load profiles and reference rotation speed signals in order to record and evaluate the system response. Figures 6 and 7. show the torque and rotation speed response of the motor. The variable load consists step-like and ramp-like parts either. This result is given in normal operation of the motor at a fixed rotation speed reference signal, so the widest torque range is examined. The control circuits torque response follows the variable load fast and accurate. The rotation speed changes as expected as the load varies as the transients are short in time.

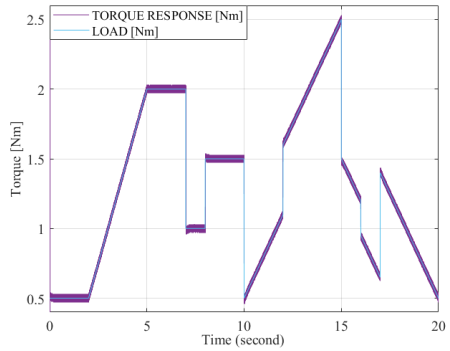

Fig. 6. Torque response in normal operation (fixed speed reference and variable load)

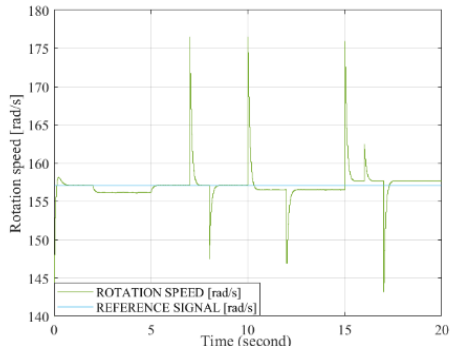

Fig. 7. Rotation speed response in normal operation (fixed speed reference and variable load)

Figure 8 shows the rotation speed response of the motor. The variable rotation speed reference consists step-like and ramp-like parts either. This result is given in normal operation of the motor at a fixed load. The system responds to the change in the rotation speed reference signal as prompt and precise as awaited. The reference signal covers a wide range so that way the maximal speed can be determined. As the motor reaches its maximal speed there is a transient in the control that is because of the overshoot of the reference signal that the integral component of the PI controller accumulates. This type of inaccuracy can be eliminated by limiting the reference signal. Figure 9 is the diagram of the motor torque in the same simulation. Compared to Figure 11 which shows the motor torque in field weakening operation it can be seen from the spikes that the control circuit is more sensitive in the latter case.

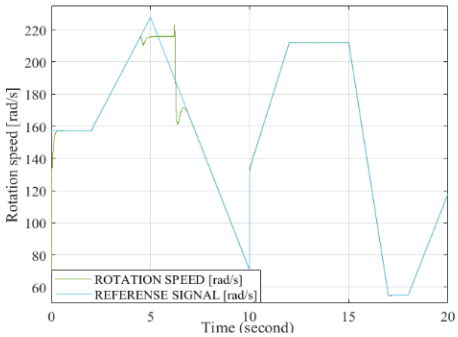

Fig. 8. Rotation speed response in normal operation (variable speed reference and fixed load)

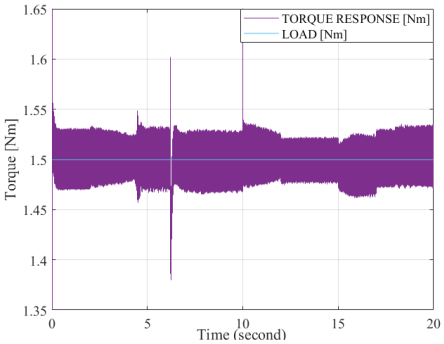

Fig. 9. Torque response to variable speed in normal operation (variable speed reference and fixed load)

Figure 10 shows the speed response of the motor defined by test parameters. This result is given in field weakening operation of the motor at a fixed load. Figure 11 is the diagram of the motor torque in the same simulation. As the field weakening is enabled in the system, it can be clearly seen that the range of the rotation speed is wider. There is a blackspot in the control as the rotation speed is near to the maximum speed of the normal operation. It may be caused by the mistuning of parameter M or the enabler relay.

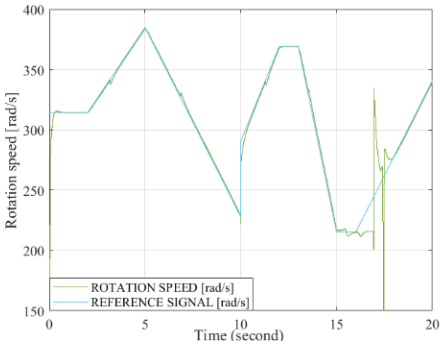

Fig. 10. Rotational speed response in field weakening operation (variable speed reference and fixed load)

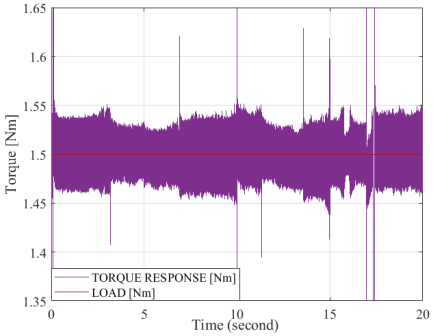

Fig. 11. Torque response to variable speed in field weakening operation (variable speed reference and fixed load)

Figure 12 shows the T(ω) characteristic of the system. It clearly defines the normal and the field weakening operation range of the interior permanent magnet synchronous motor (IPM) used as a basis for the simulations and a reference to validate the results. A slight wave in the simulation result can be seen due to the different resolution of the curves as the simulation is created by a vector with element number 200 in addition the reference curve consists only 20.

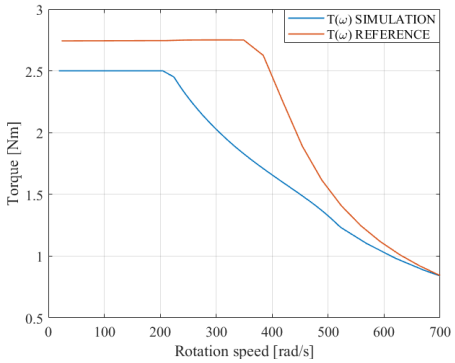

Fig. 12. T(ω) characteristic of the system

5. Conclusion and further investigation

The goal of this simulation is to get the T(ω) characteristic of the reference motor. As it can be seen there is a difference between the reference and the simulated results. There are two main reasons behind that. The motor model used in Simulink is an analytical model that utilizes constant parameters from the FEMM simulations given at a constant current. The parameters are highly dependent on the current and the load angle. This fact is not taken into consideration in the motor model. One further improvement is to use parameter matrices to utilize the result from FEMM simulations and to implement the current and load angle dependence. On the other hand, the represented control method could be improved as well, especially focusing on the field weakening operation range. To further utilize the capability of the finite element calculations, it is suitable to use maximum torque per ampere (MTPA) or maximum torque per volt (MTPV) control strategies. This assumes further improvements in the finite element calculations to get the $T(i_d, i_q)$ map of the motor topology. To summarize it, the control circuits torque response follows the variable load fast and accurately. The system responds to the change in the rotation speed reference signal as prompt and precise as expected.

By using the Figure 12 it can be decided if the designed concept can be used in an electric vehicle as its operational range meets the expectations. By implementing the equations summarized in the previous chapters, the entire electric powertrain of a vehicle can be modelled by determining the required boundary conditions. The results confirm that this model is a good starting point to perform further simulations at different operation cases. With further improvements and the verification of the model the design of a unique motor might be commenced. A specified model can greatly facilitate the early validation of expected measurement results. With the help of software suitable for finite element calculations it is possible to examine any motor topology, to determine the set of parameters that can serve as input values of the previously presented model. Using the characteristics specified by the manufacturers of the selected materials, the electrical losses can be approximated, furthermore a complete driving cycle can be examined, and the efficiency map can be drawn.

To reach the goal to create a software code which can assist the optimization of the design process of an electric motor the following investigation and improvements have to be carried out. During doctoral studies I would like to improve the utilization of finite element calculations, combine those fully with the complex powertrain presented in this paper. I hope, that experimental data based on measurements will be available for the model verification too. It is important to take advantage of cutting-edge technology with applying sufficient computer capacity to find the best solution in all cases. I think this research can help to create a cleaner future through e-mobility.

Acknowledgement

I would like to thank for the help of Vilmos Paiss and Gábor Vörös in the field of finite element calculations and Árpád Handler and Tibor Vajsz PhD. in the field of motor control. The research reported in this paper and carried out at the BME has been supported by the NRDI Fund based on the charter of bolster issued by the NRDI Office under the auspices of the Ministry for Innovation and Technology.

References

[1] **Katona M., Radnai R.:** *Primary energy consumption and CO2 emission of internal combustion engine and electric vehicles*. 6th International Youth Conference on Energy (IYCE), Budapest, 2017, pp. 1-5, doi: 10.1109/IYCE.2017.8003720., 2017

[2] **Adamas Intelligence:** *Rare Earth Magnet Market Outlook to 2030 - Executive summary report - Q3 2020* Published at august 2020

[3] **Pillay P., & Krishnan R.:** *Modeling of permanent magnet motor drives.* IEEE Transactions on Indus-trial Electronics, 35(4), 537–541. doi:10.1109/41.9176, 1988

[4] **Vajsz T., Rácz Gy., Számel L.:** *Novel modified dtc-svm method with better overload-capability for permanent magnet synchronous motor servo drives.* Periodica Polytechnica, Electrical Engineering and Computer Science. 61. 253-263. 10.3311/PPee.10428., 2017

[5] **Vajsz T., Számel L.:** *An investigation of robust speed-controllers for permanent magnet synchronous motor servo drives.* Conference: Automation and Applied Computer Science Workshop (AACS), 2015

[6] **Schmidt I., Veszprémi K.:** *Drive Control,* Budapest University of Technology and Economics Department of Electric Power Engineering,

[7] **Kuslits M.:** *Állandómágneses szinkrongépek modellalapú irányításfejlesztése,* Publio Kiadó Kft. ISBN: 978-963-424-879-8 2016

[8] **Haugen, F.:** *The Good Gain method for simple experimental tuning of PI controllers.* Modeling, Identification and Control, Vol. 33, No. 4, 2012, pp. 141–152, ISSN 1890–1328, 2012

[9] **Ziegler, J. G., Nichols N. B.:** *Optimum settings for automatic controllers*, trans. ASME 64.11 1942